vehicles

MDPI

Article

Protective Materials and Cold-Side Airflow Effects on a Thermoelectric Generator for Automotive Exhaust Energy Recovery

George Achitei *, Lamara Achitei, Aristotel Popescu, Daria Sachelarie, Lidia Gaiginschi, Teodor Anita and Elena Adelina Chiriac

Department of Automotives and Mechanical Engineering, Faculty of Mechanics, "Gheorghe Asachi" Technical University of Iasi, 61–63 Mangeron Blvd, 700050 Iasi, Romania; lamara.achitei@academic.tuiasi.ro (L.A.); aristotel.popescu@academic.tuiasi.ro (A.P.); daria.sachelarie@academic.tuiasi.ro (D.S.); lidia.gaiginschi@academic.tuiasi.ro (L.G.); teodor.anita@student.tuiasi.ro (T.A.); elena-adelina.chiriac@student.tuiasi.ro (E.A.C.)

* Correspondence: george.achitei@academic.tuiasi.ro

Abstract

Waste heat recovery from automotive exhaust gases represents an important strategy for improving vehicle energy efficiency. This study experimentally investigates the performance of a thermoelectric generator (TEG) system based on TEC1-12706 modules running under different cold-side cooling conditions and incorporating a Hot Rolled Steel (HRS) protective layer on the hot side. The HRS plate was used to ensure uniform heat distribution and protect the thermoelectric module against thermal shocks generated by a 250 °C heat source. Four cooling regimes were experimentally analyzed: natural convection and forced airflows equivalent to 40, 60, and 90 km/h. The results proved that increasing airflow intensity significantly improved the temperature difference across the module, from approximately 16 ± 2 °C under natural convection to nearly 40 ± 2 °C at the highest airflow velocity. Correspondingly, the steady-state voltage generated increased from approximately 0.25 ± 0.01 V to over 0.60 ± 0.01 V under an 82 Ω resistive load. The measured hot-side temperature remained below 75 °C in all experimental conditions, confirming the thermal protection capability of the HRS layer. The experimental data also revealed a near-linear relationship between voltage and temperature difference, consistent with the Seebeck effect. The proposed configuration shows the feasibility of combining thermal protection and forced convection cooling to improve the stability and electrical performance of thermoelectric waste heat recovery systems intended for low-power automotive auxiliary applications.

Keywords: thermoelectric generator; waste heat recovery; thermal management; air cooling; automotive applications; thermoelectric module; Seebeck effect

Check for updates

Academic Editor: Adolfo Dannier

Received: 2 April 2026
Revised: 15 May 2026
Accepted: 19 May 2026
Published: 21 May 2026

Copyright: © 2026 by the authors. Licensee MDPI, Basel, Switzerland. This article is an open access article distributed under the terms and conditions of the Creative Commons Attribution (CC BY) license.

1. Introduction

Energy recovery from exhaust gases represents a solid direction for improving the energy efficiency of internal combustion and hybrid vehicles, offering the potential to convert waste heat into usable electrical energy without extreme modifications to the engine [1]. Thermoelectricity is based on the Seebeck effect to perform the direct conversion of a temperature difference into electrical voltage. Thermoelectric (TE) technologies have attracted increasing interest due to the absence of moving parts and their high potential

reliability. For instance, Lan et al. [2] demonstrated the feasibility of using vehicular TEGs not only for exhaust waste heat recovery but also for engine oil warm-up, highlighting their multifunctional potential. Achitei et al. [3] provided a detailed analysis of the current state-of-the-art and future trends within the automotive industry, while a more recent comprehensive review by Achitei et al. [4] discussed the critical integration strategies and materials necessary for successful implementation in modern vehicle architectures.

However, the practical use of TE converters remains limited by several interdependent factors. One primary challenge is the relatively low performance of TE materials, which are quantified by the dimensionless figure of merit,

$$ZT = \frac{\alpha^2 \cdot \sigma \cdot T}{\kappa} \quad (1)$$

where α is the Seebeck coefficient, σ is the electrical conductivity, κ is the thermal conductivity, and T is the absolute temperature. Beyond material limits, efficiency is heavily influenced by the heat exchanger design. For instance, Luo et al. [5] demonstrated that an optimal heat exchanger design is crucial for passenger car applications to maximize heat capture. Furthermore, the same research group [6] explored performance improvements by extending the hot-side area using heat pipes, highlighting the importance of effective thermal management in these systems.

Furthermore, the trade-offs between energy gain and aerodynamic or exhaust back pressure penalties make the design of an ATEG (Automotive Thermoelectric Generator) a multidisciplinary problem that combines thermophysics, mechanical design, and electrical systems engineering [7].

A key element in maximizing the performance of a TEG is the optimization of the hot side heat exchanger between the hot gas flow and the TE module surface. Recent designs have demonstrated that enhanced structures, such as wavy fins, integrated vapor chambers, or annular/coaxial configurations, can increase the effective heat transfer area while reducing pressure losses. For instance, Luo et al. [5] developed an optimal heat exchanger design specifically for passenger car TEG systems to maximize heat capture. Complementing this, the comprehensive review by Pandey and Hansdah [8] categorizes various heat exchanger geometries and highlights how these advanced configurations lead to significant increases in the power available for conversion.

On the cold side, the efficient management of thermal flux is equally critical, as maintaining a low temperature for the radiator or heat-sink allows the maximization of the temperature difference (ΔT) across the terminals of the TE module and, implicitly, the generated power. Research has shown that various integration strategies can produce substantial improvements in system performance. For instance, Luo et al. [6] demonstrated that extending the hot-side area of the heat exchanger using heat pipes significantly enhances heat recovery. In parallel, Zhao et al. [9] conducted an experimental study on intermediate fluid thermoelectric generators, showing that optimized thermal delivery and adapted geometries are crucial for stabilizing the thermoelectric characteristics under variable loads.

Intermediate materials and architectures, including thermal contact plates, high-temperature protection layers, and sealing materials—play a significant role in the long-term stability of TE systems mounted in the aggressive exhaust environment. The correct material selection can reduce TE module degradation, improve local heat transfer, and limit corrosion or mechanical degradation under cyclic operation [10,11].

Regarding practical applications, experimental work and feasibility studies have provided valuable data on the recoverable energy potential and the remaining weaknesses: real-world performance depends heavily on operating conditions (speed, engine load,

thermal regime), the efficiency of the heat exchanger, and the capacity of auxiliary systems to maintain an effective cold temperature at the bottom of the TE module [12,13].

Beyond traditional exhaust applications, thermoelectric principles are applied in diverse thermal environments. For instance, Gizicki and Malecha [14] experimentally demonstrated the recovery of cold exergy from Liquefied Natural Gas (LNG) using TEGs, showcasing the technology's potential under cryogenic conditions. Similarly, optimization of the heat source is critical; recent numerical investigations into micro-combustors with advanced geometries [15] provide vital insights into enhancing system performance through improved thermal management.

Recent development directions in the field focus on multiple optimization layers. For instance, Shahrudin and Ahmad [16] verified the practical usage of Peltier modules as electric generators for vehicles, emphasizing the need for higher ZT materials. Regarding thermal architecture, the work of Martins et al. [17] remains a benchmark for using heat pipes to provide adaptive temperature control and extend the contact surface. Furthermore, Mohammed et al. [18] recently conducted an experimental analysis showing that these systems must be designed to optimize performance according to driving conditions while minimally penalizing the exhaust flow rate and fuel economy.

Recent literature indicates that the recovery potential is real, but practical exploitation on a commercial scale requires simultaneous optimization of materials, thermal interfaces, and cold-side thermal management. Pandey and Hansdah [8] emphasized that the heat exchanger design is the primary driver for efficiency, while Mohammed et al. [18] demonstrated the direct correlation between TEG integration and improved fuel economy in internal combustion engines. Furthermore, a comprehensive review by Yang et al. [19] spans the entire scale of TEG applications, from micropower to kilowatt systems, highlighting the importance of system-level optimization. Practical challenges under various operating conditions were experimentally investigated by Gao et al. [20], whereas Silva [21] provided fundamental insights into the heat transfer mechanisms between the exhaust pipe and the thermoelectric modules. Thus, effective solutions must combine these material innovations with heat dissipation designs that maintain a high ΔT under real-world driving conditions.

The novelty of this study lies in the combined experimental investigation of a protective hot-side material (Hot Rolled Steel—HRS) and controlled cold-side airflow under multiple operating conditions. Unlike previous studies that typically focus either on thermoelectric material performance or heat exchanger optimization independently, this work evaluates the interaction between thermal protection and forced convection cooling within a unified experimental framework. HRS offers a balance of moderate thermal conductivity and high thermomechanical stability, acting as a thermal damper to protect standard TEC1-12706 modules from thermal shocks. The novelty of this work lies in the experimental validation of this configuration under simulated automotive cooling conditions (up to 90 km/h), providing a practical engineering solution for increasing the lifespan and reliability of waste heat recovery systems.

Furthermore, the study is based on a highly repeatable experimental methodology, involving multiple test repetitions for each operating regime, ensuring consistent and reliable results. The integration of thermal imaging for validating heat transfer behavior represents an additional contribution, providing insight into temperature distribution and system stability.

This approach offers new perspectives on the role of intermediate materials and cooling strategies in enhancing the performance and reliability of thermoelectric generators for automotive waste heat recovery applications.

2. Protective Materials

In automotive exhaust waste heat recovery (WHR) applications, the use of a protective layer interposed between the thermal source (e.g., exhaust pipe, heat exchanger plate) and the thermoelectric module (TEM) represents a strategic design decision. The primary purpose of the protective material is to provide a controlled environment for heat transfer and protection, with multiple benefits for the system's performance, durability, and safety [22,23].

The protective material fulfills critical functions: thermal insulation and limiting heat losses to the environment, ensuring a uniform temperature distribution at the interface between the hot plate and the TEM, physical and chemical protection of TEM against vibrations, thermal shocks, or direct contact with exhaust gases, and acting as a barrier that allows the exploitation of higher temperatures without degrading sensitive elements [23].

A material with low thermal conductivity acts as a thermal buffer, maintaining a larger ΔT (temperature difference) between the hot and cold faces of TEM, thus increasing the potential for electrical generation [1]. The selection criteria include high-temperature stability, a low coefficient of thermal expansion (CTE), resistance to oxidation, mechanical compatibility with the contact plates, and an optimal thickness that balances insulation and thermal transfer [22].

The integration of protective material brings direct benefits to TEG performance:

- Maintaining the temperature difference, as limiting heat losses from the hot side maximizes the thermal difference between the faces, which is essential in automotive applications [22].
- Thermal distribution uniformity: the protective layer attenuates "hot spots" and improves thermal stability [23].
- Mechanical and thermal protection: since automotive environment involves vibrations, corrosion, and thermal shocks, the protective material acts as a structural barrier [24].
- Tolerance to high temperatures to allow operation at higher temperatures without TEM degradation, increasing the converted energy [1].

The use of protective material also involves trade-offs:

- Optimal thermal conductivity: a layer that is too insulating reduces heat transfer to the TEM, while a too conductive one does not offer adequate protection [23].
- Weight and volume, as additional mass can influence the exhaust flow and overall efficiency [1].
- Thermomechanical compatibility: the material must withstand repeated temperature cycles without losing thermal contact [24].
- Cost and durability: high-performance materials can be expensive or difficult to integrate on an industrial scale [1].

For the experimental stand designed for energy recovery from exhaust gases, a plate made of Hot Rolled Steel (HRS) was selected to be used as the protective layer situated between the thermal source and the thermoelectric module. This choice is based on an optimal combination of thermal, mechanical, and structural integration properties, which make HRS a suitable solution for the specific experimental environment. A decisive factor in the selection is the moderate thermal conductivity of HRS—values for carbon steel have been reported in the range of 45–58 W/m·K, depending on the heat treatment and microstructure of the material [25]. This intermediate value provides a balance between efficient heat transfer and thermal flux control, allowing for a gradual dissipation of thermal energy and reducing the phenomenon of "thermal shock" at the module interface. In contrast, materials with much higher conductivities (e.g., copper, aluminum) would transfer heat excessively fast, risking localized overheating, while materials with much lower conductivity would limit useful transfer and reduce the ΔT available to the module.

HRS exhibits stable thermomechanical behavior at high temperatures and under repeated thermal cycles—an essential parameter in a testing environment where the hot and variable airflow (simulated by the air gun) imposes rapid temperature changes. Studies on hot-rolled steel have demonstrated that the resulting microstructure provides predictable thermal expansion, good dimensional stability, and favorable mechanical resistance to vibrations and thermal stresses [26]. In the context of automotive thermoelectric applications, these properties contribute to maintaining effective thermal contact and preventing premature module degradation.

Furthermore, the HRS plate serves as structural support and physical protection: it provides a robust metallic base that withstands the stresses of the experimental environment (high temperatures, variable airflows, repeated mechanical contact), while also ensuring a sufficiently conductive surface to transfer heat to the thermoelectric module. Additionally, since metal plates usually constitute common elements in the architecture of automotive exhaust systems, the use of HRS allows for good compatibility with the rest of the experiment's components, avoiding the need for special adaptations and facilitating mechanical reproducibility.

In conclusion, the HRS plate was selected as the protective layer due to:

- Moderate thermal conductivity, which controls the heat flow and maintains the ΔT capable of generation.
- Thermomechanical stability at high temperatures and rapid thermal cycles, ensuring durability under testing conditions.
- Structural compatibility with the experimental environment and ease of integration into a simulated automotive system.

This combination of characteristics gives the HRS material a key role in ensuring system performance and the stability of experimental data.

3. General Role of Cooling in TEGs

Cooling plays an essential role in the overall performance of a thermoelectric generator (TEG). From a physical standpoint, the efficiency of energy conversion in a TEG module directly depends on the temperature difference (ΔT) between the hot and cold surfaces. Therefore, optimizing the cold-side cooling system becomes crucial for increasing the heat flux through the device and, implicitly, the generated electrical power [27].

3.1. Thermal Gradient Importance

The performance of a TEG is determined by maintaining the largest possible thermal difference between the module's two faces. Heat from the hot source must be efficiently transferred to the thermoelectric material, while the cold side must be kept at a low temperature through an adequate thermal dissipation mechanism. If the cooling system is insufficient, the thermal gradient drops rapidly, which reduces the Seebeck voltage and the conversion efficiency [28].

In automotive applications, where temperature variations can be abrupt, the thermal stability of the cold side is essential not only for performance but also for the protection of sensitive components. Recent studies have shown that efficient cold-side temperature control can increase the generated electrical power by 20–40% compared to operation without active cooling [29].

3.2. Passive Cooling Systems (Natural Convection)

Passive cooling systems, based on natural convection, are frequently used in laboratory applications and small-scale prototypes. They have the advantage of zero auxiliary energy consumption, being silent and easy to implement. However, the overall heat transfer

coefficient achieved through natural convection is limited (approximately 5–25 W/m·K, which renders this type of cooling insufficient in high heat flux applications [30].

3.3. Forced Air Cooling and Automotive Integration

Forced cooling represents the preferred solution in most automotive TEG applications, as it allows for better control of the thermal flux. Air is directed through radiators, heat sinks, or aerodynamically optimized channels, ensuring a rapid removal of thermal energy from the cold side of the module [31].

In recent literature, experiments conducted at equivalent air speeds between 40 km/h and 100 km/h have demonstrated a substantial increase in generated power, due to the intensification of convection and the maintenance of a high thermal gradient [32].

At the same time, the integration of a forced cooling system into the vehicle's architecture must be achieved without significant penalties on overall aerodynamics or auxiliary energy consumption. A comparative study highlighted that using forced air directed from the engine fan can improve TEG's performance without significantly affecting the vehicle's overall energy efficiency [33,34].

The efficiency of the cooling system is a critical element in determining the TEG performance, as it directly influences the heat flux evacuated from the cold side and, implicitly, the magnitude of the temperature difference. Recent literature clearly shows that maintaining a low temperature on the cold side can improve electrical production by substantial percentages, depending on the cooling configuration used [35,36].

A fundamental aspect in evaluating cooling efficiency is the ratio between the energy recovered by the TEG and the energy consumption of the auxiliary system. According to Cho's study [35], if the energy consumed by the cooling system exceeds 10–15% of the energy generated, the overall efficiency becomes unjustified for real integration. This is crucial in automotive applications, where auxiliary energy resources are carefully optimized.

Optimizing the efficiency of the cooling process requires a careful balance between thermal performance and constraints imposed by system construction. Studies indicate that optimized radiator fin architecture, characterized by thin and densely packed fins, can lead to an increase in thermal system dissipation in the range of 15–25%, without implying additional energy consumption. Concurrently, the implementation of aerodynamic ducting for the controlled direction of the air current significantly contributes to improving convective heat transfer, while also ensuring better thermal stability on the cold side of the system. Zebarjadi et al. highlighted that efficient thermal management on the cold side improves module stability and reduces the microstructural degradation of thermoelectric materials [37].

Cooling system efficiency must be viewed as the result of a compromise between thermal performance, auxiliary energy cost, and the impact on the overall device design. A high-performing TEG system is not the one that cools the most aggressively, but the one that ensures an optimal balance between thermal dissipation, energy consumption, system reliability, and physical integration into the existing configuration. In the present study, the variation in air speed (0, 40, 60 and 90 km/h) allows for the direct investigation of these compromises, providing a clear picture of how the intensification of cooling influences the thermal gradient and the measured electrical performance.

4. Experimental Setup and Methodology

This section presents the experimental configuration utilized for evaluating the performance of the thermoelectric generator (TEG) under control conditions, including variations in the cooling airflow and the use of a protective material (HRS plate) on the hot side.

The methodology includes both the structural description of the experimental prototype and the procedures used for data acquisition, covering temperature measurements, generated voltage, and thermal behavior of the system. In addition, aspects related to measurement repeatability, uncertainty estimation, and thermal validation are addressed to ensure the reliability of the experimental results.

The configuration of the test stand is shown in Figure 1, and the main elements are described hereafter.

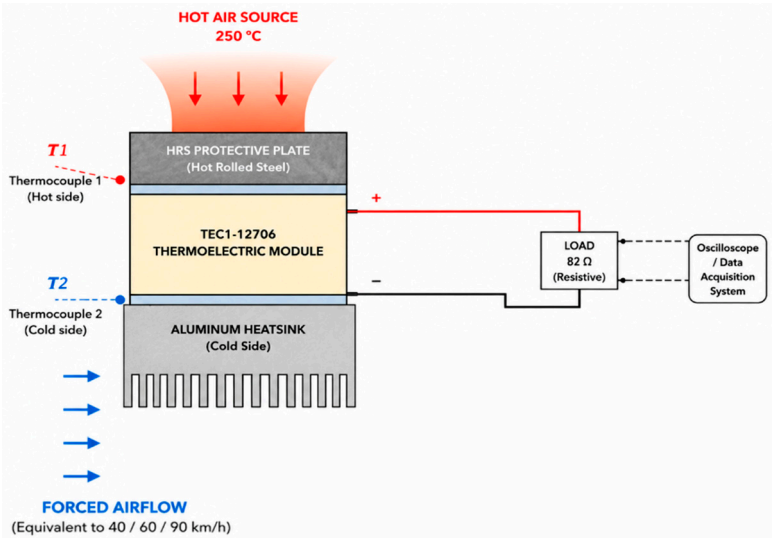


Figure 1. Schematic representation of the experimental thermoelectric generator setup, including the HRS protective layer, TEC1-12706 module (commercially available model, China), aluminum heatsink, thermocouples (T1 and T2), heat source, and forced airflow direction.

The experimental setup was configured in a layered stack (sandwich) to ensure optimal heat flow. The heat source was in direct contact with the HRS plate (buffer), followed by the TE module, and finally the aluminum heat sink. All interfaces were treated with thermal grease to minimize contact resistance. Temperature monitoring was performed using Type-K thermocouples placed at the hot-side interface (T1) and the cold-side base of the radiator (T2).

4.1. Structural Configuration of the TEG Prototype

The experimental configuration used in the tests was designed to reproduce, in a controlled environment, the operating conditions of a TEG system mounted on an exhaust pipe. The assembly is built on a rigid platform, using a modular structural frame made of aluminum profiles, which allows for the quick repositioning of components depending on the test geometry. The main geometric dimensions and material characteristics of the experimental assembly are summarized in Table 1.

Table 1. Geometric and material specifications of the experimental assembly.

Component	Material	Dimensions/Specifications
Protective Plate	Hot Rolled Steel (HRS)	45 mm × 45 mm × 2 mm
TE Module	Bismuth Telluride (Bi2Te3)	TEC1-12706 (40 mm × 40 mm × 3.6 mm)
Heat Sink (Radiator)	Aluminum Alloy	Length: 45 mm; width: 45 mm; total height: 30 mm; fin height: 26.4 mm; fin thickness: 1.4 mm; fin spacing: 3.51 mm; base thickness: 3.6 mm
Thermal Interface	Silicone-based Grease	Thermal conductivity: >1.5 W/mK

The assembly consists of three main components, arranged in layers:

- Hot-Side Protective Layer: A plate made of Hot Rolled Steel (HRS) was mounted on the upper side of the system, acting as a protective material and as an element for uniform temperature distribution. This plate served as the interface with the heat source, contributing to the maintenance of thermal stability and protecting the Peltier module against rapid thermal shocks, generating a controlled thermal flux toward the device's active area. The HRS plate was used in its untreated commercial condition, without additional surface coating or polishing.
- Thermoelectric Module (TEM): A Peltier-type thermoelectric module (TEC1-12706 commercially available model, China) was installed in the central position, dimensioned to operate under a temperature difference regime. The module was connected to the data acquisition system for real-time measurement of the generated voltage and current. The TEC1-12706 module was selected for this experimental study due to its wide commercial availability, low cost, compact dimensions, and predictable thermoelectric behavior under moderate temperature gradients. While high-temperature Bi2Te3 or skutterudite modules are more commonly used in advanced automotive exhaust recovery systems, the use of a standard Peltier module allowed for a controlled evaluation of the HRS plate's protective capabilities as a thermal buffer. This approach provides a baseline for future transitions to industrial-grade thermoelectric modules while minimizing experimental costs during the validation of the protective assembly. A single thermoelectric module was intentionally used in this study in order to isolate and evaluate the individual influence of thermal protection and forced cooling conditions on the thermoelectric response.
- Cold-Side Heat Dissipation: An aluminum heatsink was mounted on the lower side of the device, featuring vertical fins, designed for efficient heat dissipation when cold air is directed onto it. The heatsink geometry was chosen to maximize convection under forced flow conditions.

Instrumentation was integrated to control and monitor key parameters:

- Heat Source Simulation: A hot air gun with temperature control (Parkside PHLGB 2000 A1, Neckarsulm, Germany) was used to simulate thermal energy from exhaust gases. The thermal jet was oriented directly onto the HRS plate, with the source positioned at an approximate distance of 1 cm from the surface. The temperature of the hot side was monitored continuously.
- Cold Source Simulation (Forced Cooling): A cold air blower (Hilti NBL 6-22, Schaan, Liechtenstein) was utilized on the cold side of the TEG, capable of generating controlled airflow velocities. The blower was positioned such that the airflow was directed primarily toward the heatsink, ensuring controlled cooling conditions and minimizing external disturbances.
- Temperature Measurement: The stand is equipped with a calibrated digital thermometer connected to two K-type thermocouples (Tektronix DTM920, Beaverton, OR, USA). The thermocouples were positioned at the interfaces between the thermoelectric module and the contact materials, ensuring direct thermal contact and accurate measurement of the hot-side (T1) and cold-side (T2) temperatures.
- Voltage Measurement: A digital oscilloscope (FNIRSI-1014D, Shenzhen FNIRSI Technology Co., Ltd., Shenzhen, China) was used for voltage measurement. This allowed for the measurement of the instantaneous voltage generated by the Peltier module during the tests and the possibility of analyzing waveforms, signal stability, and voltage evolution as a function of temperature variation.
- Electrical Load Configuration: The electrical circuit included a fixed resistive load of 82 Ω. This load was intentionally selected to operate the thermoelectric module

under a low-current quasi open-circuit regime, allowing stable voltage monitoring and comparative analysis of the thermal behavior under different cooling conditions. The objective of the present study was not to maximize electrical power extraction, but rather to evaluate the feasibility of using the proposed TEG configuration for low-power auxiliary automotive applications, such as signal lighting or low-consumption electronic systems.

- Air Speed Measurement: Anemometer (HABOTEST HT605, Habotest Technology Co., Ltd., Shenzhen, China) was used to measure the actual speed of the airflow generated by the blower, thereby confirming the set values for the four test scenarios (0, 40, 60 and 90 km/h). This instrument enabled the precise quantification of the cold airflow interacting with the heatsink and the lower side of the thermoelectric module, ensuring that each test was performed at a stable and well-defined speed.
- Thermal Monitoring: A thermal camera (Hilti PT-C, Schaan, Liechtenstein) was used to monitor the temperature distribution on the HRS plate and the heatsink. This allowed visualization of heat transfer processes, verification of temperature uniformity, and identification of potential thermal losses within the system.

The four experimental regimes were:

- Test 1: No airflow (natural convection);
- Test 2: Airflow equivalent to 40 km/h;
- Test 3: Airflow equivalent to 60 km/h;
- Test 4: Airflow equivalent to 90 km/h.

These speeds were calibrated using a digital anemometer placed directly in front of the heatsink, ensuring accuracy in establishing the testing conditions.

4.2. Experimental Procedure and Data Acquisition

The experimental tests were conducted using the developed test stand under controlled laboratory conditions, following a well-defined procedure to ensure consistency and reproducibility of the results. For each operating regime, all experimental parameters were maintained constant, with the only variable being the airflow velocity applied for cooling the cold side of the thermoelectric module.

The experimental procedure began with the activation of the heat source, consisting of a hot air gun set to a constant temperature of 250 °C. The device was positioned at an approximate distance of 1 cm from the HRS plate. It should be noted that the temperature of the hot air source does not correspond directly to the temperature measured at the thermoelectric module interface, due to the thermal buffering effect provided by the HRS protective layer. Prior to data acquisition, the system was allowed to preheat for approximately 30 s to ensure stabilization of the thermal input on the hot side. Following the preheating stage, the cold air blower was activated to simulate cooling conditions relevant to automotive applications. For each test, the airflow velocity was adjusted to the desired values (0, 40, 60, and 90 km/h) and continuously monitored using an anemometer positioned near the experimental assembly to ensure stable and controlled conditions. The hot-side temperature (T1) and cold-side temperature (T2) were measured using K-type thermocouples, positioned at the interfaces between the thermoelectric module and the contact materials to ensure accurate thermal readings. The temperature difference (ΔT) was monitored in real time and used as a key parameter for evaluating system performance.

The electrical voltage generated by the thermoelectric module was measured using a digital oscilloscope, within an electrical circuit incorporating a fixed resistive load of 82 Ω. This configuration enabled the evaluation of the module under realistic operating conditions, avoiding open-circuit measurements.

Each test was carried out over a total duration of 600 s. To ensure data accuracy and consistency, the entire experimental process was recorded using video from two different angles. The recorded data were subsequently analyzed, and the values of temperature, temperature difference, and voltage were extracted at regular intervals of 15 s. This approach minimized reading errors and allowed for a detailed assessment of the temporal evolution of the measured parameters.

During the experiments, a rapid increase in the hot-side temperature was observed during the initial phase, followed by a gradual stabilization of the temperature difference as the cold side progressively warmed due to heat transfer. The steady-state regime was reached when the variations in temperature difference became minimal and remained relatively constant over an extended period.

To evaluate the repeatability and reliability of the experimental results, each operating condition was tested multiple times, with over 20–30 repetitions performed for each airflow regime. The analysis of these repeated tests showed a high level of consistency, with only minor variations observed between measurements, particularly in the steady-state regime. Based on this consistency, representative datasets were selected for analysis, corresponding to the tests that most accurately reflect the general behavior observed throughout the experimental campaign. The experimental variability observed between repeated measurements remained relatively small, particularly in the steady-state regime. Therefore, representative error bars corresponding to the measurement uncertainty and repeatability were included in the temperature difference plots.

The measurement uncertainties were estimated based on the specifications of the instruments used in the experimental setup. The K-type thermocouples used for temperature measurements have an accuracy of approximately ± 1 °C, while the voltage measurements obtained using the digital oscilloscope present an estimated uncertainty of ± 0.01 V. The airflow velocity, monitored using the anemometer, has an estimated uncertainty of ± 2 km/h. Considering these factors, the overall uncertainty associated with the temperature difference (ΔT) is estimated to be within ± 2 °C, which is acceptable for experimental evaluation of thermoelectric systems.

In addition, thermal validation of the experimental setup was performed using a thermal imaging camera. This allowed real-time visualization of the heat transfer process, verification of temperature distribution uniformity, and identification of potential heat losses. The thermographic analysis confirmed the proper thermal behavior of the system and supported the reliability of the measured data.

This comprehensive experimental methodology ensures the acquisition of consistent, reliable, and representative results for the evaluation of thermoelectric generator performance under different cooling conditions.

Although real automotive exhaust systems may operate at significantly higher temperatures depending on engine load and combustion conditions, the present experimental configuration was intentionally designed as a controlled laboratory-scale validation platform focused on evaluating the thermal protection capability of the HRS layer and the influence of cold-side airflow on thermoelectric behavior.

5. Results and Discussion

The experimental results are presented for the four investigated cooling regimes, highlighting the influence of airflow intensity on the thermal gradient and electrical response of the thermoelectric module. For each regime, the system exhibited a transient phase followed by a quasi-steady-state behavior, where the temperature difference and generated voltage remained within a relatively narrow range. The reported values correspond to representative datasets, selected based on the repeatability of the experimental results.

This section presents a detailed analysis of the experimental results obtained from evaluating the TEC1-12706 SR thermoelectric module, conducted under controlled temperature conditions.

The use of the thermal camera allowed for a qualitative visual assessment of the temperature distribution on the surface of the Hot Rolled Steel (HRS) plate and the heatsink, providing an additional perspective on the uniformity of heat transfer and the efficiency of cold-side heat dissipation. Figure 2 depicts representative thermal images for the four experimental regimes, highlighting how the intensity of forced cooling influences the overall thermal gradient.

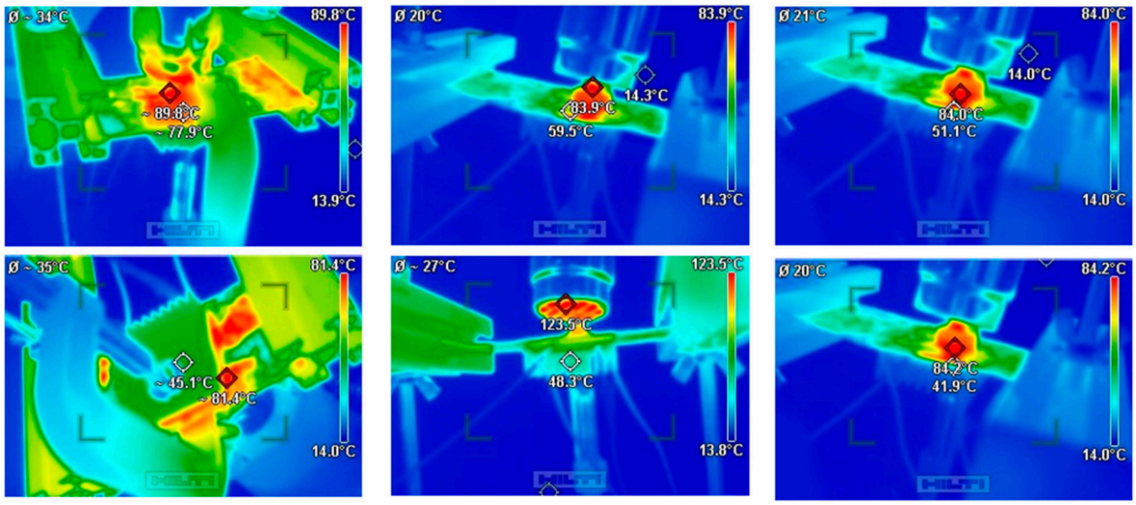


Figure 2. Temperature variations monitored on the thermal camera.

Table 2 summarizes the representative steady-state temperatures measured on the hot side (T1) and cold side (T2) of the thermoelectric module under different cooling conditions. Although the hot air source temperature was maintained at 250 °C, the temperatures measured at the module interface remained significantly lower due to the thermal buffering effect of the HRS plate. The results confirm that the protective layer effectively limited the thermal stress applied to the TEC1-12706 module while maintaining a sufficient temperature gradient for thermoelectric generation. The measured hot-side temperatures remained below 75 °C in all experimental regimes, indicating that the thermoelectric module operated within a safe thermal range throughout the tests. Furthermore, the increase in airflow intensity contributed to a significant reduction in the cold-side temperature (T2), leading to a substantial increase in the overall temperature difference across the module.

Table 2. Representative steady-state temperatures measured under different cooling conditions.

Cooling Condition	T1 (°C)	T2 (°C)	ΔT (°C)
Natural convection (0 km/h)	74.3	58.5	15.8
Forced cooling—40 km/h	68.7	37.9	30.8
Forced cooling—60 km/h	69.7	34.9	35.2
Forced cooling—90 km/h	69.5	30	39.5

5.1. Test 1: No Airflow

Figure 3 illustrates the thermal behavior of the system under conditions where no forced airflow was applied. The evolution of the temperature difference (ΔT) reflects the combined effect of heat accumulation and limited natural heat dissipation on the cold side.

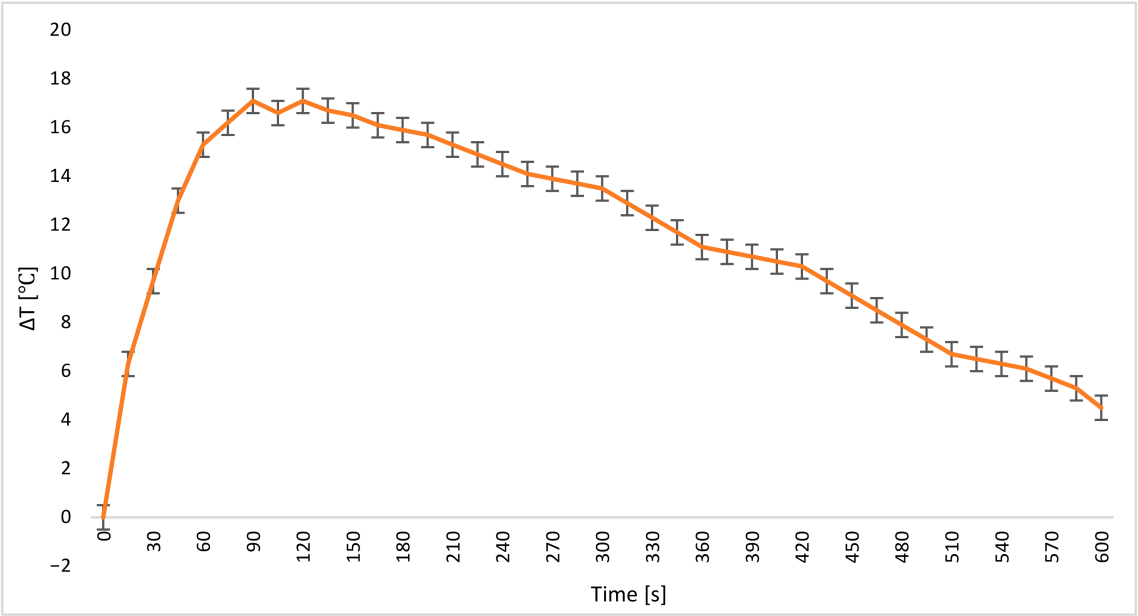


Figure 3. Evolution of the temperature difference under natural convection conditions. Error bars represent the estimated experimental uncertainty and repeatability of the measurements.

In the initial phase (0–90 s), ΔT increases rapidly, reaching a peak value of approximately 16–17 °C. This behavior indicates that the hot side of the module heats up significantly faster than the cold side, which relies solely on natural convection for heat dissipation. During this stage, thermal accumulation dominates, and the system has not yet reached any form of equilibrium.

After reaching the maximum value, the temperature difference begins to gradually decrease over time. This decline is clearly visible throughout the interval from approximately 120 s to 600 s, where ΔT continuously drops to values around 4–5 °C. This behavior suggests that heat progressively accumulates on the cold side, reducing the effectiveness of the thermal gradient. Unlike an ideal steady-state regime, where ΔT would stabilize, the observed trend indicates that the system is unable to maintain a constant thermal gradient under natural convection conditions. The decrease in ΔT can be attributed to insufficient heat dissipation from the cold side, leading to a gradual thermal equalization between the two surfaces.

This behavior highlights a major limitation of the system operating without forced cooling: although a significant temperature difference can be initially generated, it cannot be sustained over time. As a result, the electrical performance of the thermoelectric module is negatively affected, emphasizing the necessity of active cooling solutions for maintaining stable and efficient operation.

Figure 4 illustrates the variation in the voltage generated by the thermoelectric module as a function of the temperature difference under natural convection conditions. A rapid increase in voltage is observed as ΔT rises from 0 °C to approximately 16–17 °C, reaching peak values of around 0.24–0.25 V.

After reaching the maximum, the voltage gradually decreases as ΔT declines, dropping to approximately 0.05 V for temperature differences around 4–5 °C. This trend indicates that the system cannot sustain a stable voltage under natural convection conditions, due to insufficient heat dissipation on the cold side. These results highlight the importance of maintaining a stable thermal gradient for consistent thermoelectric performance.

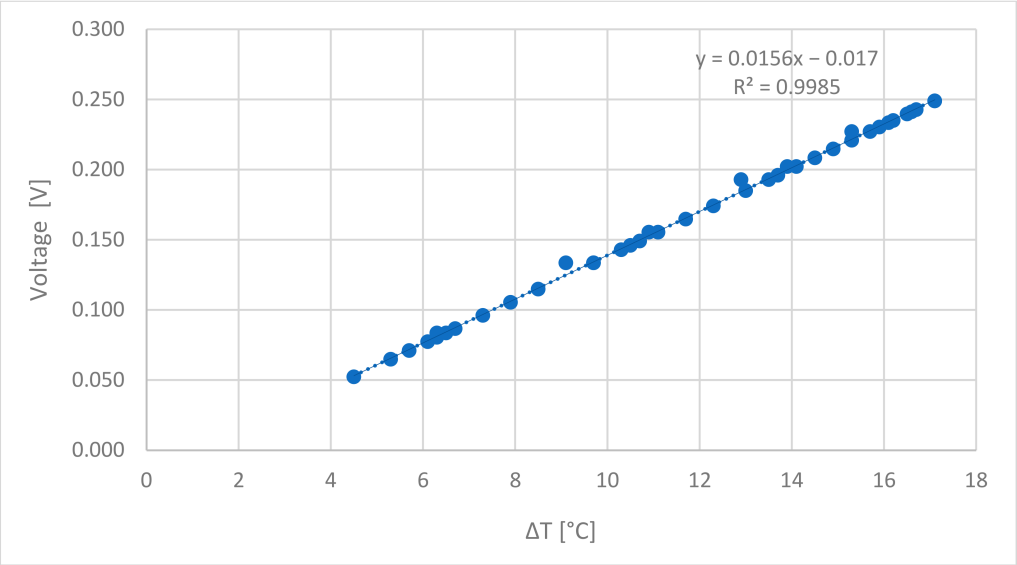


Figure 4. Relationship between generated voltage and temperature difference under natural convection conditions. The linear regression trendline highlights the near-linear thermoelectric response consistent with the Seebeck effect.

5.2. Test 2: Airflow Equivalent to 40 km/h

The evolution of the temperature difference from Test 2 indicates the thermoelectric response of the system when the cold side is subjected to a low velocity forced airflow (40 km/h). Figure 5 illustrates the evolution of the temperature difference under forced cooling conditions corresponding to an airflow equivalent to 40 km/h. Immediately after applying the heat source, ΔT exhibits a rapid increase in the first 60–90 s, reaching values exceeding 25 °C. This accelerated increase is characteristic of the transient regime, where the hot side (the HRS plate heated with hot air) stabilizes its thermal conductivity, while the cold side begins to be influenced by the forced convection generated by the blower.

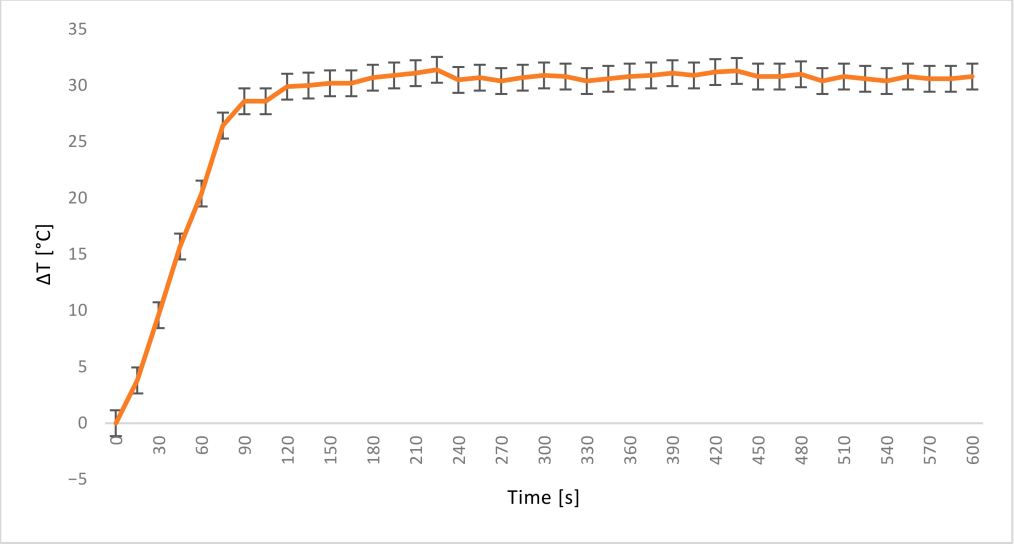


Figure 5. Evolution of the temperature difference under forced cooling conditions at an airflow equivalent to 40 km/h. Error bars represent the estimated experimental uncertainty and repeatability of the measurements.

In the 90–150 s interval, the graph shows a transition toward the quasi-steady-state regime, with temperature differences stabilizing in the 28–30 °C range. This indicates that

a 40 km/h cooling airflow improves heat transfer on the cold side compared to conditions without airflow, but it is not intense enough to cause a rapid drop in heatsink temperature. According to the literature, at low air speeds, the heat transfer coefficient increases only moderately (approx. 30–50 $W/m^2 \cdot K$), leading to a thermal equilibrium where the heatsink can evacuate heat, but with limited efficiency [35].

Test 2 demonstrates that a low airflow produces a significant increase in ΔT compared to the natural cooling condition, confirming the importance of forced convection in creating a stable and efficient thermal gradient for TEGs. The system stabilizes quickly and offers superior thermal performance, indicating that this cooling regime is sufficient to ensure efficient operation without excessive energy consumption.

The curve of the generated voltage as a function of the temperature difference (Figure 6) for the low forced cooling regime—40 km/h highlights the typical thermoelectric behavior of a TEG module subjected to a thermal flux stabilized by controlled cold air circulation. The voltage increases rapidly and almost linearly in the initial zone as ΔT rises from 0 to approximately 20–25 °C, confirming the directly proportional relationship between ΔT and the generated voltage, as described in specialized literature for Bi_2Te_3-based modules.

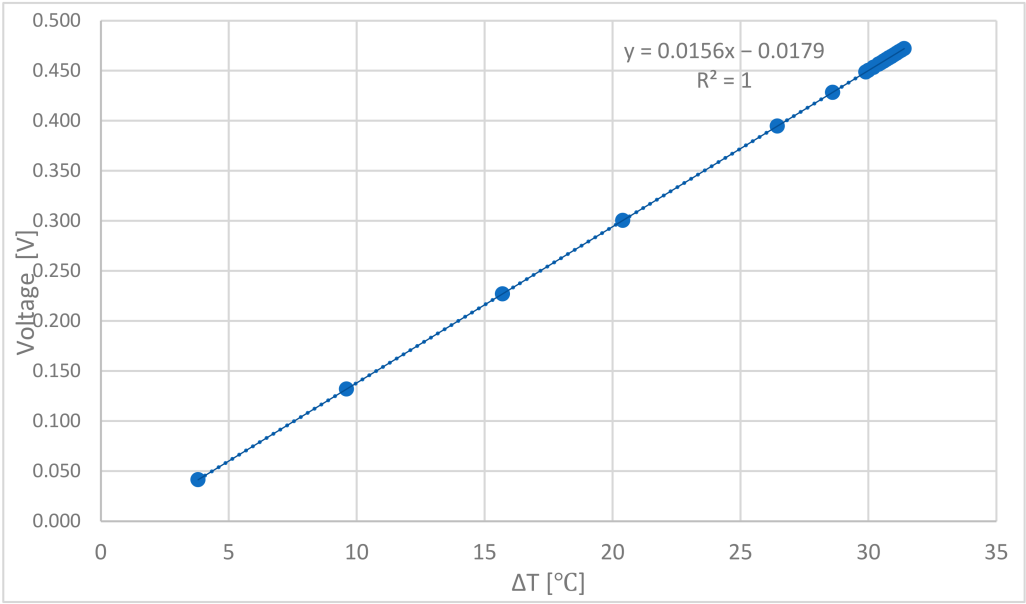


Figure 6. Relationship between generated voltage and temperature difference under forced cooling conditions at an airflow equivalent to 40 km/h. The linear regression trendline highlights the near-linear thermoelectric response consistent with the Seebeck effect.

The graph clearly illustrates the critical role of airflow in stabilizing and increasing the temperature difference across the thermoelectric module's terminals. Forced cooling at 40 km/h ensures the necessary conditions for obtaining a higher ΔT and a significantly superior maximum voltage compared to the test without forced air, confirming the effectiveness of moderate convective cooling in TEG applications.

5.3. Test 3: Airflow Equivalent to 60 km/h

Figure 7 corresponding to Test 3 highlights the evolution of the temperature difference over 600 s under conditions of a forced cold airflow of 60 km/h, representing an intermediate cooling scenario. The curve indicates a rapid increase in ΔT in the first 75–90 s, a period during which the system reaches the transient regime characteristic of the initial thermal load. The ΔT value increases from 0 to approximately 32–33 °C, due to the simultaneous

application of hot airflow on the upper side and the intensification of dissipation on the cold side via the blower.

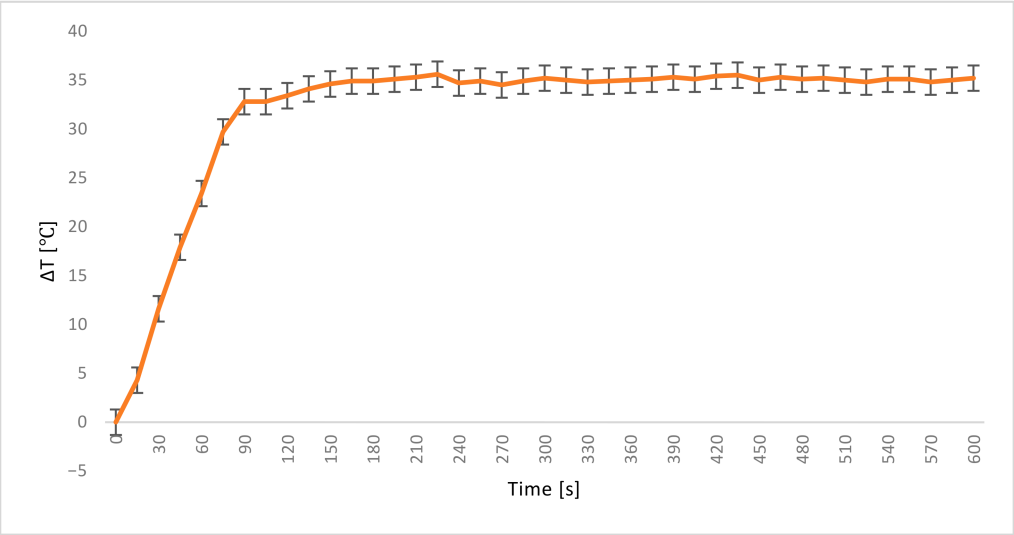


Figure 7. Evolution of the temperature difference under forced cooling conditions at an airflow equivalent to 60 km/h. Error bars represent the estimated experimental uncertainty and repeatability of the measurements.

Subsequently, after approximately 120 s, a transition into the quasi-steady-state regime is observed, where ΔT stabilizes within the range of 34–36 °C. The small variations in the curve (±0.5 °C) are attributed to natural fluctuations in the aerodynamic flow and the thermal inertia of the conductor-heatsink assembly. The stabilization of ΔT at higher values than those measured in Test 2 confirms that the increase in air speed improves the convective heat transfer coefficient on the cold side, thereby reducing the heatsink temperature and increasing the overall temperature gradient applied to the TEG module. This behavior is consistent with results reported in specialized literature, where the intensification of forced convection leads to a direct increase in the evacuated thermal flux and, implicitly, the amplification of the useful ΔT [31].

The experimental data obtained in Test 3 shows an almost ideal evolution of the thermoelectric voltage as a function of the temperature difference (Figure 8), characterized by a rapid increase in the initial phase and subsequent stabilization around a maximum value of approximately 0.53–0.55 V. At the medium airflow speed 60 km/h, the cooling is sufficiently intense to maintain ΔT in the 34–35 °C range, which stabilizes the voltage on a plateau with minimal variations. This behavior indicates that the performance limit is no longer determined by the cooling, but rather by the internal properties of the TEG module and the total thermal resistance of the assembly.

5.4. Test 4: Airflow Equivalent to 90 km/h

Figure 9 illustrates the evolution of the temperature difference under forced cooling conditions corresponding to an airflow equivalent to 90 km/h. The increase in airflow speed to 90 km/h leads to the highest temperature difference obtained among all tests, with ΔT reaching ~40 °C after approximately 120–150 s. The intensified forced cooling rapidly stabilizes the thermal regime, and after the transient phase, ΔT remains almost constant with minor oscillations (<1 °C), indicating a well-controlled quasi-steady-state regime. This behavior confirms that an increased convective coefficient allows for the efficient extraction of heat from the cold side, maximizing the thermal gradient and, implicitly, the generation potential of the TEG module, consistent with results reported in the specialized literature.

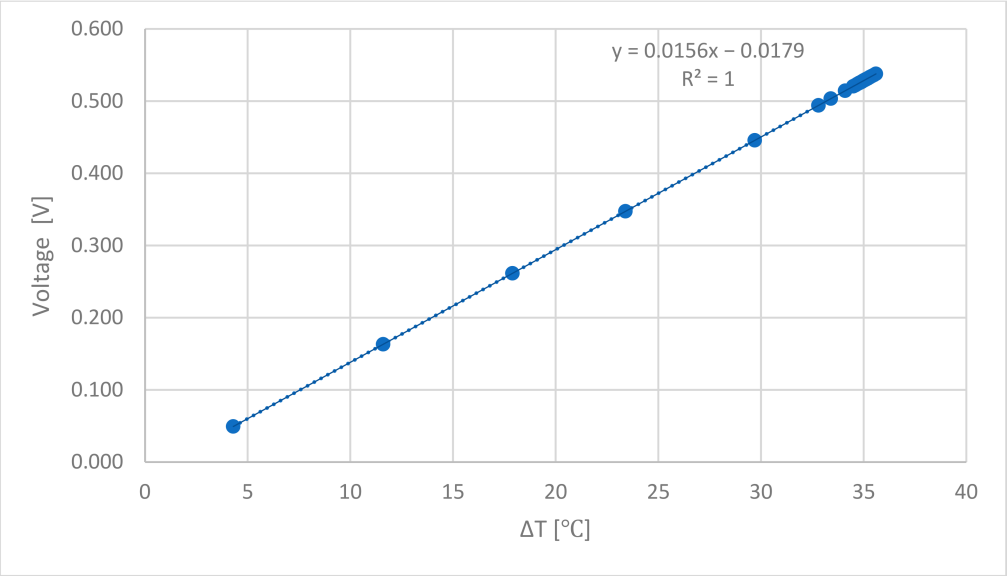


Figure 8. Relationship between generated voltage and temperature difference under forced cooling conditions at an airflow equivalent to 60 km/h. The linear regression trendline highlights the near-linear thermoelectric response consistent with the Seebeck effect.

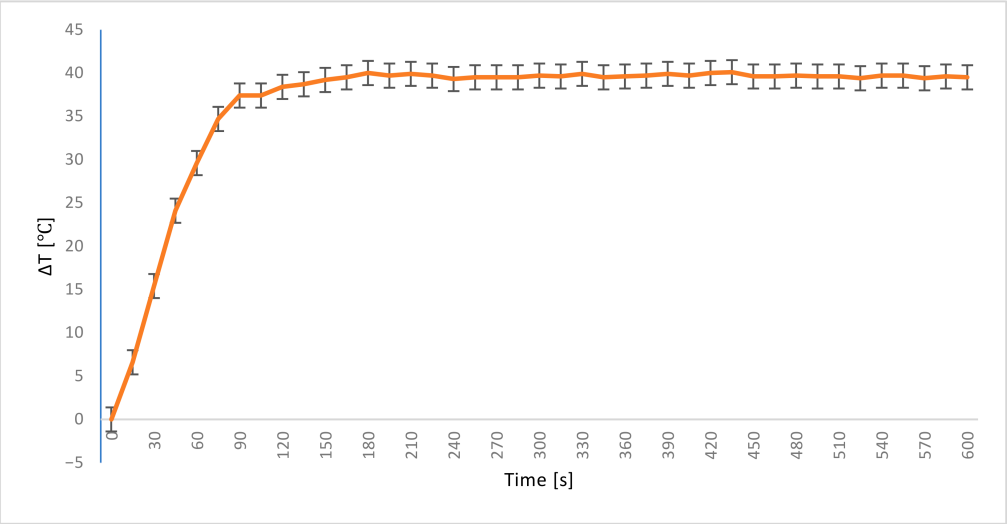


Figure 9. Evolution of the temperature difference under forced cooling conditions at an airflow equivalent to 90 km/h. Error bars represent the estimated experimental uncertainty and repeatability of the measurements.

Figure 10 shows an almost linear relationship initially between the increase in the temperature difference (ΔT) and the voltage generated by the TEG module, followed by a saturation zone. As ΔT rapidly increases towards ~35–40 °C, the voltage rises from 0 to approximately 0.60 V, reaching the plateau characteristic of the steady-state regime. This stabilization suggests that, at the high airflow speed (90 km/h), the intensified cooling reduces the thermal resistance of the heatsink and maximizes the thermal gradient, allowing the TEG to operate close to its optimal heat transfer point.

Figure 11 clearly demonstrates the progressive increase in the temperature difference with increasing airflow intensity, confirming the dominant influence of forced convection on cold-side thermal management.

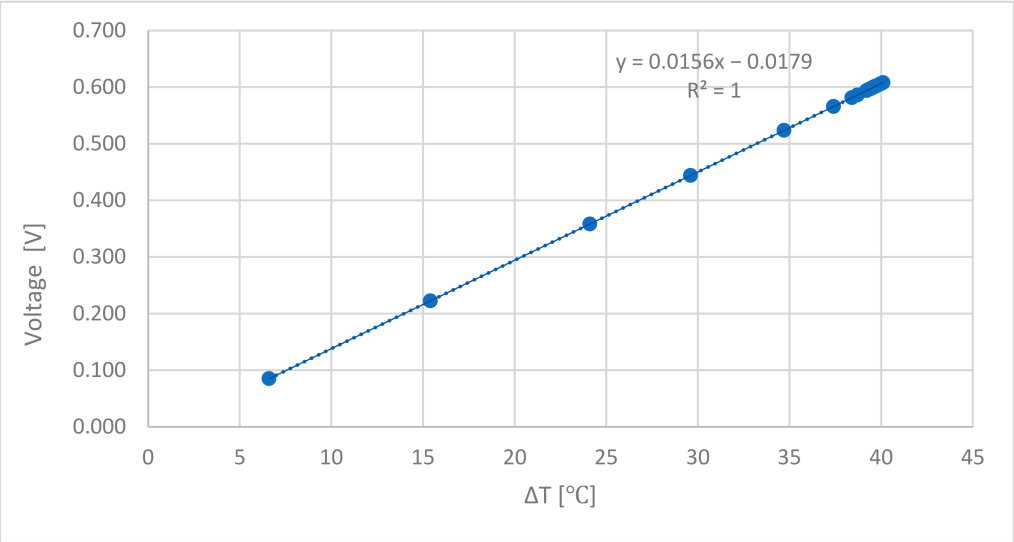


Figure 10. Relationship between generated voltage and temperature difference under forced cooling conditions at an airflow equivalent to 90 km/h. The linear regression trendline highlights the near-linear thermoelectric response consistent with the Seebeck effect.

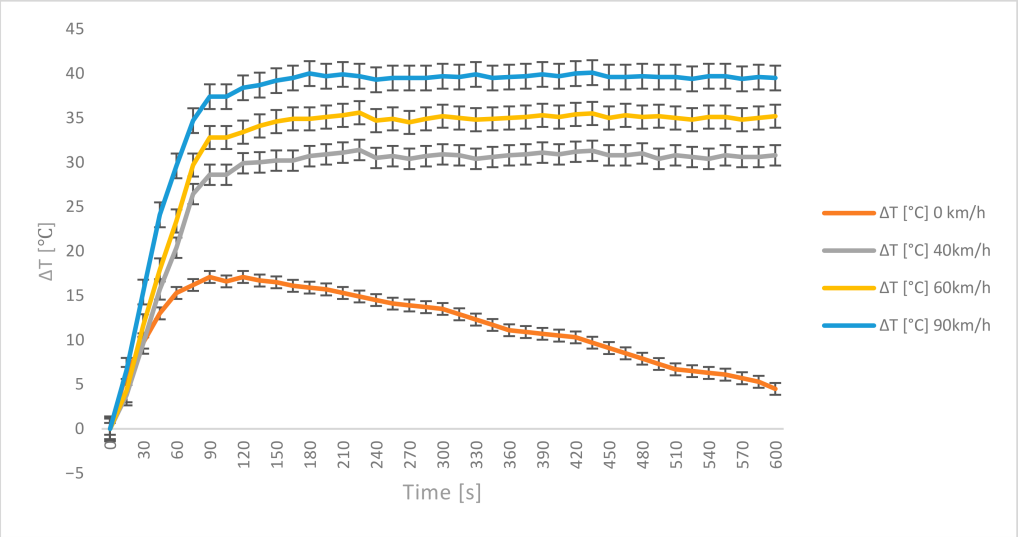


Figure 11. Comparative evolution of the temperature difference under different cooling airflow regimes.

The comparative analysis of the evolution of the temperature difference for the four cooling scenarios—0 km/h, 40 km/h, 60 km/h and 90 km/h—confirms the determining role of forced convection in stabilizing and intensifying the thermal flux through the TEG module. In the absence of airflow, ΔT only reaches 16–17 °C before stabilizing, indicating limited thermal dissipation on the cold side and a rapid increase in heatsink temperature, a phenomenon specific to the regime dominated by natural convection.

The introduction of an airflow of 40 km/h causes an abrupt increase in ΔT up to approximately 30–31 °C, due to the intensification of the overall heat transfer coefficient and the accelerated heat evacuation from the heatsink.

At 60 km/h, ΔT stabilizes in the 34–36 °C range, further increasing the efficiency of thermal dissipation and significantly reducing the total thermal resistance of the system.

The highest-performing configuration is the one with a flow of 90 km/h, where ΔT reaches values on the order of 38–40 °C, remaining constant throughout the test duration.

This evolution confirms that the intensification of forced convection increases the thermal gradient applied to the TEG module, leading to a more stable thermal flux and a superior thermoelectric conversion potential.

The general trend observed—a rapid increase in ΔT in the first 60–120 s followed by a stabilization at a plateau characteristic of each speed—is consistent with specialized literature, where the performance of TEGs increases with the reduction in the heatsink temperature and the maintenance of a high and stable ΔT in the quasi-steady-state regime. The differences between the four curves confirm that the efficiency of thermal management increases almost linearly in relation to the speed of the cooling fluid, with evident benefits for the operation of the thermoelectric module.

5.5. Interpretation of Results

The experimental results demonstrate that forced cooling plays a critical role in stabilizing the thermal behavior of the thermoelectric generator and maintaining a sufficiently high temperature difference for efficient electrical generation. Under natural convection conditions, the temperature difference gradually decreased due to heat accumulation on the cold side and limited heat dissipation. Consequently, the generated voltage also decreased over time, confirming the direct relationship between thermal gradient stability and thermoelectric performance.

The thermoelectric performance of the system can be interpreted based on the Seebeck effect, which establishes a direct relationship between the temperature difference (ΔT) and the generated voltage (V):

$$V = S \cdot \Delta T \tag{2}$$

where S represents the Seebeck coefficient of the thermoelectric material.

The experimental voltage data exhibited a near-linear dependence on the temperature difference, consistent with the expected Seebeck behavior of the thermoelectric module.

As observed in Figures 4, 6, 8 and 10, this proportional relationship is clearly reflected in the experimental data. Deviations from ideal linearity in the steady-state regime can be attributed to internal electrical resistance, thermal losses, and contact resistance within the system. The high values of the regression coefficient (R^2) confirm the strong linear correlation between voltage generation and temperature difference under all investigated cooling conditions.

The experimental behavior observed in this study is consistent with the fundamental thermoelectric theory, confirming that enhanced cooling directly improves the electrical response of the module by increasing the temperature difference across the thermoelectric junctions. In addition to the voltage analysis, the electrical power generated by the thermoelectric module was estimated to use the measured voltage values and the known resistive load (R = 82 Ω), based on the relation:

$$P = \frac{V^2}{R} \tag{3}$$

Using this approach, the power output was found to increase significantly with the intensification of forced cooling.

Table 3 summarizes the steady-state electrical performance obtained under different cooling conditions. The calculated electrical power output increased significantly with airflow intensity due to the enhanced temperature difference established across the thermoelectric module. The highest power levels were obtained under forced cooling conditions, reaching approximately 4.39 mW at airflow regimes equivalent to 60 km/h and 90 km/h. Although the absolute power values remained relatively low under the selected high-resistance operating conditions, the results demonstrate the feasibility of low-power

energy harvesting for auxiliary automotive applications. Furthermore, the results indicate that intensified cold-side cooling plays a dominant role in improving the thermoelectric response of the proposed TEG configuration.

Table 3. Steady-state electrical performance under different cooling conditions.

Cooling Condition	Steady-State Voltage (V)	Load Resistance (Ω)	Calculated Power Output (mW)
Natural convection (0 km/h)	0.249	82	0.756
Forced cooling—40 km/h	0.473	82	2.73
Forced cooling—60 km/h	0.600	82	4.390
Forced cooling—90 km/h	0.600	82	4.390

Although the selected load resistance is significantly higher than the internal resistance of the TEC1-12706 module, the adopted configuration was considered appropriate for the objectives of this study. The experimental setup was designed primarily to investigate the influence of thermal protection and forced cooling on voltage stability and thermoelectric response, rather than to determine the maximum electrical power output under impedance-matching conditions. The obtained voltage levels demonstrate the feasibility of supplying low-power automotive auxiliary systems, particularly when multiple thermoelectric modules are connected in series.

Although the absolute power values obtained in this study are relatively low, they are consistent with the performance of small-scale thermoelectric modules operating under moderate temperature gradients. The results demonstrate that electrical output is strongly influenced by the effectiveness of the thermal management system. The increase in airflow intensity significantly enhances heat dissipation on the cold side, leading to a higher temperature difference and improved electrical performance. This highlights the critical role of cooling strategies in optimizing thermoelectric generator efficiency in automotive applications. Therefore, even under controlled laboratory conditions, the results confirm the practical potential of integrating thermoelectric systems for waste heat recovery, provided that thermal management is properly optimized.

The experimental results confirm that both forced cooling intensity and the HRS protective layer play essential roles in the thermal and electrical stability of the proposed TEG configuration. Increasing the airflow velocity improved heat dissipation on the cold side, resulting in higher and more stable temperature differences across the module. Consequently, the generated voltage and calculated power output increased significantly under forced cooling conditions. In parallel, the HRS layer ensured a more uniform heat transfer from the hot source to the thermoelectric module, limiting localized overheating and contributing to the stability and repeatability of the measurements. These findings demonstrate that simultaneous optimization of thermal protection and cold-side cooling is essential for improving the performance and durability of thermoelectric waste heat recovery systems intended for automotive applications.

A comparative analysis of the experimental results indicates a clear correlation between airflow intensity and thermoelectric performance. The temperature difference increased from approximately 16 °C under natural convection to nearly 40 °C at the highest airflow velocity. Correspondingly, the generated voltage increased from approximately 0.22 V to values exceeding 0.60 V.

The variations observed during the steady-state regime remained relatively small (typically within ±1 °C for temperature difference and ±0.02 V for voltage), confirming the stability of the system and the reliability of the measurements. These results prove that

forced convection significantly enhances the thermal gradient and, so, the electrical output of the thermoelectric module.

A direct experimental comparison with alternative interface materials or with the absence of a protective layer was beyond the scope of the present study. However, based on the observed thermal stability and the moderate thermal conductivity of HRS, the selected configuration proved suitable for protecting the thermoelectric module while supporting a sufficient temperature gradient. Future investigations will include comparative analyses using alternative metallic interfaces and direct hot-side exposure conditions.

6. Conclusions

The experimental study demonstrated the combined influence of the HRS protective layer and forced air cooling on the thermal and electrical performance of the proposed thermoelectric generator configuration for automotive waste heat recovery. The HRS plate ensured uniform heat distribution and effectively limited the hot-side temperature at the thermoelectric module interface to values below 75 °C, despite the 250 °C heat source applied during testing.

The results confirmed that forced cooling on the cold side significantly improves the temperature difference across the module and stabilizes the thermoelectric response. The measured temperature difference increased from approximately 16 °C under natural convection to nearly 40 °C at the highest airflow velocity, while the generated voltage increased from approximately 0.25 V to over 0.60 V.

The experimental findings demonstrate the feasibility of combining thermal protection and forced convection cooling to improve the stability and electrical performance of thermoelectric waste heat recovery systems. The proposed configuration provides a practical and low-cost approach for enhancing thermoelectric operation under automotive-like thermal conditions. These results support the potential integration of thermoelectric generators into future vehicle energy recovery architectures, particularly for low-power auxiliary applications.

The present study primarily focused on the thermal stability and electrical response of the proposed TEG configuration. A comprehensive thermal efficiency and exhaust energy recovery analysis under real engine operating conditions will be addressed in future investigations.

7. Future Work

Future development directions of this study aim to extend the system to real operating conditions and optimize the thermoelectric architecture for automotive applications. The first step involves scaling the prototype and integrating it into an experimental vehicle to evaluate the TEG's performance under real exhaust gas flows, dynamic driving conditions, and thermal load variations specific to urban and extra-urban cycles.

In parallel, advanced numerical simulation of temperature distribution and thermal fluxes is necessary using CFD methods (Computational Fluid Dynamics) and multi-layer thermal modeling. The goal is to optimize the positioning of protective materials, the contact geometry between metal plates and the TEG, and the efficiency of cooling systems. These models can contribute to identifying configurations with minimal losses and maximum heat transfer.

Another essential direction is the improvement of cold-side thermal management, a critical aspect for increasing the temperature difference and implicitly the generated power. Investigating hybrid cooling architectures, materials with high conductivity, or optimized heatsink structures can lead to superior thermal stability and higher overall efficiency.

Future investigations will also include experiments performed under impedance-matching conditions using lower external load resistances, allowing the evaluation of maximum power output and conversion efficiency under optimized electrical operating conditions. This approach will provide a more detailed assessment of the practical energy recovery capability of the proposed thermoelectric configuration for automotive applications.

Furthermore, the development of a complete Power Electronics and Energy Management (PEEM) module is indispensable for harnessing the recovered energy. This involves DC-DC circuits optimized for low currents, MPPT systems (Maximum Power Point Tracking) dedicated to TEGs, and the integration of the recovered energy into the vehicle's electrical network or storage systems.

Future investigations will also include comparative experimental analyses using alternative interface materials, such as copper and aluminum plates, as well as direct hot-side exposure configurations without a protective layer, in order to further evaluate the influence of interface thermal properties on TEG stability and performance.

Through these research directions, the analyzed TEG system can evolve toward a robust and scalable solution for thermal energy recovery in automotive applications, contributing to increased energy efficiency and reduced emissions.

Author Contributions: Conceptualization, A.P., L.G., L.A., G.A., D.S., T.A. and E.A.C.; methodology, G.A. and L.A.; validation, A.P. and L.G.; formal analysis, D.S., T.A. and E.A.C.; investigation, L.A., G.A., D.S., T.A., E.A.C., A.P. and L.G.; resources, A.P. and L.G.; data curation, G.A. and T.A.; writing—original draft preparation, L.A.; writing—review and editing, A.P., L.G., G.A. and L.A.; visualization, D.S. and E.A.C.; supervision, A.P. and L.G. All authors have read and agreed to the published version of the manuscript.

Funding: This research received no external funding.

Data Availability Statement: The original contributions presented in this study are included in the article. Further inquiries can be directed to the corresponding author.

Acknowledgments: During the preparation of this manuscript, the authors used an artificial intelligence tool (ChatGPT (OpenAI, GPT-5)) to assist in the conceptualization of some schematic figures. The authors reviewed and edited the generated material and took full responsibility for the final content of the manuscript.

Conflicts of Interest: The authors declare no conflicts of interest.

Abbreviations

The following abbreviations are used in this manuscript:

TEG	Thermoelectric Generator
HRS	Hot Rolled Steel
TE	Thermoelectric technologies
ZT	Figure of merit
ATEG	Automotive Thermoelectric Generator
WHR	Waste heat recovery
TEM	Thermoelectric Module
CTE	Coefficient of thermal expansion
ΔT	Temperature difference
CFD	Computational Fluid Dynamics
PEEM	Power Electronics and Energy Management
MPPT	Maximum Power Point Tracking

References

1. Wang, Y.; Wang, R.; Chai, R.; Ding, R.; Ye, Q.; Sun, Z.; Meng, X.; Sun, D. Review of Automotive Thermoelectric Generator Structure Design and Optimization for Performance Enhancement. *Processes* **2025**, *13*, 1931. [CrossRef]
2. Lan, S.; Smith, A.; Stobart, R.; Chen, R. Feasibility study on a vehicular thermoelectric generator for both waste heat recovery and engine oil warm-up. *Appl. Energy* **2019**, *242*, 273–284. [CrossRef]
3. Achitei, G.; Dontu, A.I.; Chiriac, B.; Popescu, A. *State-of-the-Art and Future Trends of Thermoelectric Generation Systems in Automotive Industry*; Springer: Cham, Switzerland, 2023; pp. 1–8. [CrossRef]
4. Achiţei, L.; Achiţei, G.; Sachelarie, D.; Popescu, A. Thermoelectric Generators in Automotive Applications: A Comprehensive Review of Concepts, Materials, and Integration Strategies. *Bull. Polytech. Inst. Iaşi Mach. Constr. Sect.* **2025**, *71*, 103–114. [CrossRef]
5. Luo, D.; Wu, Z.; Yan, Y.; Ji, D.; Cheng, Z.; Wang, R.; Li, Y.; Yang, X. Optimal design of a heat exchanger for automotive thermoelectric generator systems applied to a passenger car. *Appl. Therm. Eng.* **2023**, *227*, 120360. [CrossRef]
6. Luo, D.; Yang, S.; Yan, Y.; Cao, J.; Cao, B. Performance improvement of the automotive thermoelectric generator by extending the hot side area of the heat exchanger through heat pipes. *Energy Convers. Manag.* **2024**, *310*, 118472. [CrossRef]
7. Duy, D.T.; Duy, V.N.; Tan, N.T.; Dien, V.M.; Binh, P.H. A comprehensive review of advances in thermoelectric generators: Novel materials and enhanced applications for sustainable transportation. *Int. J. Thermofluids* **2025**, *25*, 100996. [CrossRef]
8. Pandey, A.; Hansdah, D. Heat exchangers for automotive exhaust thermoelectric generators: A review. *AIP Conf. Proc.* **2021**, *2341*, 030022. [CrossRef]
9. Zhao, Y.; Zhang, G.; Wen, L.; Wang, S.; Wang, Y.; Li, Y.; Ge, M. Experimental study on thermoelectric characteristics of intermediate fluid thermoelectric generator. *Appl. Energy* **2024**, *365*, 123263. [CrossRef]
10. Attar, A.; Albatati, F. Analytical and experimental investigation of thermoelectric generators for low-grade waste heat recovery from air conditioning units. *Int. Commun. Heat Mass Transf.* **2025**, *165*, 109083. [CrossRef]
11. Mahapatra, A.; Kondaguli, R.S. A Review of Thermoelectric Generators for Automotive Waste Heat Recovery Systems. *TechRxiv* **2025**. [CrossRef] [PubMed]
12. Kim, D.-H.; Seo, S.; Kim, S.; Shin, S.; Son, K.; Jeon, S.-J.; Han, S. Design and performance analyses of thermoelectric coolers and power generators for automobiles. *Sustain. Energy Technol. Assess.* **2022**, *51*, 101955. [CrossRef]
13. Balasubramanian, R. Overview of the use of Peltier's modules in technology. *Mod. Eng.* **2020**, *1*, 11–17.
14. Gizicki, W.; Malecha, Z. Experimental Analysis of LNG Cold Exergy Recovery Using Thermoelectric Generators. *Energies* **2026**, *19*, 1959. [CrossRef]
15. He, Z.; Liu, S.; Qi, W.; Song, J.; Lai, C.; Feng, S.; Fu, L.; Zhang, Y.; Zhang, C.; Wu, Y. Numerical investigation of a novel micro-combustor with geometrically stretched and twisted channels for enhanced thermo-photovoltaic system performance. *Appl. Therm. Eng.* **2026**, *291*, 130230. [CrossRef]
16. Shahrudin, M.A.F.; Ahmad, M.Z. Verifying Usage of Thermoelectric Peltier as an Electric Generator for Electric Vehicle. *Evol. Electr. Electron. Eng.* **2024**, *5*, 302–311.
17. Martins, J.; Goncalves, L.M.; Antunes, J.; Brito, F.P. *Thermoelectric Exhaust Energy Recovery with Temperature Control Through Heat Pipes*; SAE International: Warrendale, PA, USA, 2011. [CrossRef]
18. Jabbar, M.Y.; Ahmed, S.Y.; Khafaji, S.O.W. Experimental Analysis of Exhaust Energy Recovery Performance of an Internal Combustion Engine Using Thermoelectric Generators and Fuel Economy Evaluation. *Energy* **2025**, *332*, 137267. [CrossRef]
19. Yang, S.; Chen, H.; Luo, D. A Comprehensive Review of Thermoelectric Generators from Micropower Supply to Kilowatt System. *Green. Energy Fuel Res.* **2025**, *2*, 93–108. [CrossRef]
20. Gao, H.B.; Zong, S.C.; Zhang, C.W.; Li, H.J.; Huang, G.H. Experimental investigation of the performance of a thermoelectric generator at various operating conditions. *IOP Conf. Ser. Earth Environ. Sci.* **2021**, *702*, 012001. [CrossRef]
21. Silva, A.L.C. Heat transfer between an automotive exhaust and thermoelectric modules. *Rev. De Eng. Térmica* **2018**, *17*, 3–8. [CrossRef]
22. Wang, Z.H.; Ma, Y.J.; Tang, G.H.; Zhang, H.; Ji, F.; Sheng, Q. Integration of thermal insulation and thermoelectric conversion embedded with phase change materials. *Energy* **2023**, *278*, 127784. [CrossRef]
23. Deng, J.; Li, Q.W.; Xiao, Y.; Wang, C.P.; Shu, C.M. Thermal diffusivity of coal and its predictive model in nitrogen and air atmospheres. *Appl. Therm. Eng.* **2018**, *130*, 1233–1245. [CrossRef]
24. Yang, J.; Stabler, F.R. Automotive Applications of Thermoelectric Materials. *J. Electron. Mater.* **2009**, *38*, 1245–1251. [CrossRef]
25. Habchi, W.; Bair, S. The role of the thermal conductivity of steel in quantitative elastohydrodynamic friction. *Tribol. Int.* **2020**, *142*, 105970. [CrossRef]
26. MachineMFG. Understanding Thermal Conductivity of Steel: A Technical Deep Dive. 2025. Available online: https://shop.machinemfg.com/understanding-thermal-conductivity-of-steel/ (accessed on 11 December 2025).
27. Atmoko, N.T.; Jamaldi, A.; Riyadi, T.W.B. An Experimental Study of the TEG Performance using Cooling Systems of Waterblock and Heatsink-Fan. *Automot. Exp.* **2022**, *5*, 261–267. [CrossRef]

28. Tohidi, F.; Ghazanfari Holagh, S.; Chitsaz, A. Thermoelectric Generators: A comprehensive review of characteristics and applications. *Appl. Therm. Eng.* **2022**, *201*, 117793. [CrossRef]
29. Huang, K.; Yan, Y.; Li, B.; Li, Y.; Li, K.; Li, J. A Novel Design of Thermoelectric Generator for Automotive Waste Heat Recovery. *Automot. Innov.* **2018**, *1*, 54–61. [CrossRef]
30. Samal, P.; Tarai, H.; Meher, A.; Surekha, B.; Vundavilli, P.R. Effect of SiC and WC Reinforcements on Microstructural and Mechanical Characteristics of Copper Alloy-Based Metal Matrix Composites Using Stir Casting Route. *Appl. Sci.* **2023**, *13*, 1754. [CrossRef]
31. Luo, D.; Sun, Z.; Wang, R. Performance investigation of a thermoelectric generator system applied in automobile exhaust waste heat recovery. *Energy* **2022**, *238*, 121816. [CrossRef]
32. Yang, P.; Xia, Z.; Ma, L.; Chen, B.; Feng, Y.; Li, C.; Zhao, L. Direct-Connect Test of Solid Scramjet with Symmetrical Structure. *Energies* **2021**, *14*, 5589. [CrossRef]
33. Fernández-Yáñez, P.; Romero, V.; Armas, O.; Cerretti, G. Thermal management of thermoelectric generators for waste energy recovery. *Appl. Therm. Eng.* **2021**, *196*, 117291. [CrossRef]
34. Cao, Z.; Chen, T.; Shi, J.; Li, W. Enhanced performance of thermoelectric generation system by increasing temperature difference using spray cooling. *Appl. Therm. Eng.* **2024**, *252*, 123679. [CrossRef]
35. Cho, Y.H.; Park, J.; Chang, N.; Kim, J. Comparison of Cooling Methods for a Thermoelectric Generator with Forced Convection. *Energies* **2020**, *13*, 3185. [CrossRef]
36. Ma, T.; Qu, Z.; Yu, X.; Lu, X.; Wang, Q. A review on thermoelectric-hydraulic performance and heat transfer enhancement technologies of thermoelectric power generator system. *Therm. Sci.* **2018**, *22*, 1885–1903. [CrossRef]
37. Zebarjadi, M. Heat Management in Thermoelectric Power Generators. *Sci. Rep.* **2016**, *6*, 20951. [CrossRef]

Disclaimer/Publisher's Note: The statements, opinions and data contained in all publications are solely those of the individual author(s) and contributor(s) and not of MDPI and/or the editor(s). MDPI and/or the editor(s) disclaim responsibility for any injury to people or property resulting from any ideas, methods, instructions or products referred to in the content.